SACLANT ASW RESEARCH CENTRE REPORT

HIGH-FREQUENCY NORMAL-MODE CALCULATIONS IN DEEP WATER

by

Melchiorre C. FERLA, Finn B. JENSEN and William A. KUPERMAN

15 OCTOBER 1982

SACLANTCEN SR-63

HIGH-FREQUENCY NORMAL-MODE CALCULATIONS IN DEEP WATER

by

Melchiorre C. Ferla, Finn B. Jensen and William A. Kuperman

15 October 1982

This report has been prepared as part of Project 19.

APPROVED FOR DISTRIBUTION

RALPH R. GOODMAN
Director

High-frequency normal-mode calculations in deep water

M. C. Ferla, F. B. Jensen, and W. A. Kuperman[a]

SACLANT ASW Research Centre, 19026 La Spezia, Italy

A method has been developed to perform high-frequency deep-water normal-mode calculations in the multikilohertz region in water depths of the order of 5 km. The results from this technique agree with fast field program (FFP) solutions as well as with infinite-frequency solutions in the appropriate limit. The wave-theory calculations presented therefore provide a set of test cases for future numerically more efficient approximations.

PACS numbers: 43.30.Bp, 43.30.Jx, 43.20.Ks, 92.10.Vz

INTRODUCTION

There are two basic problems associated with performing high-frequency deep-water normal-mode calculations. The first problem is that in deep water the number of modes is approximately of the order of the frequency and lengthy calculations must therefore be performed. Of course, there is a regime where "uncorrected" ray theory is a good approximation and also over the last few years "corrected" ray theory[1] and ray-mode theories[2–5] have extended the applicability of the asymptotic ray formalism. The second problem is that numerical instabilities occur because the lower-order modes are "trapped" in the deep sound channel and are hence evanescent outside the channel. Under these circumstances, the eigenvalue search becomes unstable when the numerical algorithm attempts to calculate the eigenfunctions in regions from where they are essentially zero to where they have a finite value and then again back to zero. Multiple-shoot eigenvalue techniques[6] can alleviate some of these instabilities but such methods have not yet been applied to the multikilohertz region.

In this paper we present a simple, fast technique for alleviating the abovementioned problems. This technique is not limited to a specific normal-mode computer program and can be included in most existing programs, even those that use multiple-shoot techniques. In Sec. I we present the method with an example, and we compare the normal-mode results with standard ray-theory calculations. The examples presented in Sec. I also provide a set of test cases for future numerically more efficient approximations. In Sec. II, as an additional confirmation of the accuracy of this procedure, we compare our normal-mode high-frequency results with analytic ray theory (infinite frequency) solutions where, of course, normal-mode calculations do not encounter caustic problems.

I. THE METHOD

The technique we use is simply to put the mode functions to zero where they are essentially zero (by straightforward physics arguments) rather than to try to calculate small numbers. This automated precedure, which is similar to the approach used by Guthrie[7] for computing SOFAR duct modes, saves computation time and eliminates the basic instabilities.

In cases where numerical instabilities exist for the lower modes, we know that there are higher modes that are not evanescent and are easy to calculate. Therefore we start the calculation with the highest-order mode and progress downward in mode number. We test the mode functions to determine if they become evanescent by checking if and at what depths the vertical wavenumber becomes imaginary, that is, when

$$k^2(z) - k_n^2 < 0, \tag{1}$$

where $k(z)$ is $\omega/c(z)$ and k_n is the eigenvalue of the nth mode. When a mode is found to be evanescent, we know that the next lower mode will be even "more trapped" in the sound channel. We therefore reduce the size of the water column to where the last mode was evanescent and had a negligible value (in our examples 10^{-10} times the maximum amplitude). As we go down in mode number, we keep shrinking the size of the water column based on the structure of the lowest mode calculated, with the result that the calculation is both stable and fast (because we are using fewer and fewer integration points for calculating those modes that previously were the most difficult to calculate). In addition, the boundary conditions used for this numerical procedure are simplified since we require that the mode functions and their derivatives vanish at both upper and lower boundaries of the reduced region of calculation.

We have installed this deep-water high-frequency capability in a previously developed normal-mode program[8] that had already undergone extensive model/model[9] and model/data comparisons.[10] Without this technique, the highest frequency that could be used in calculating all the modes in 5-km water depth was about 200 Hz. At this frequency, both the previous method and the one described in this paper gave identical results. At higher frequencies the new technique has been checked against fast field program[11,12] (FFP) solutions.

In Fig. 1 we illustrate numerical results for a water depth of 5 km and a frequency of 3.5 kHz. Part of a typical deep-water profile is shown together with some of the resulting modes. The inner lines show where the modes have been determined to be evanescent as calculated from the above formula. The outer lines display where the water column has been automatically truncated as we go down in mode number. Propagation loss is obtained by summing all the modal contributions. Before we present the propagation-loss results, we show in Fig. 2 a ray-trace calculation[13] for a source
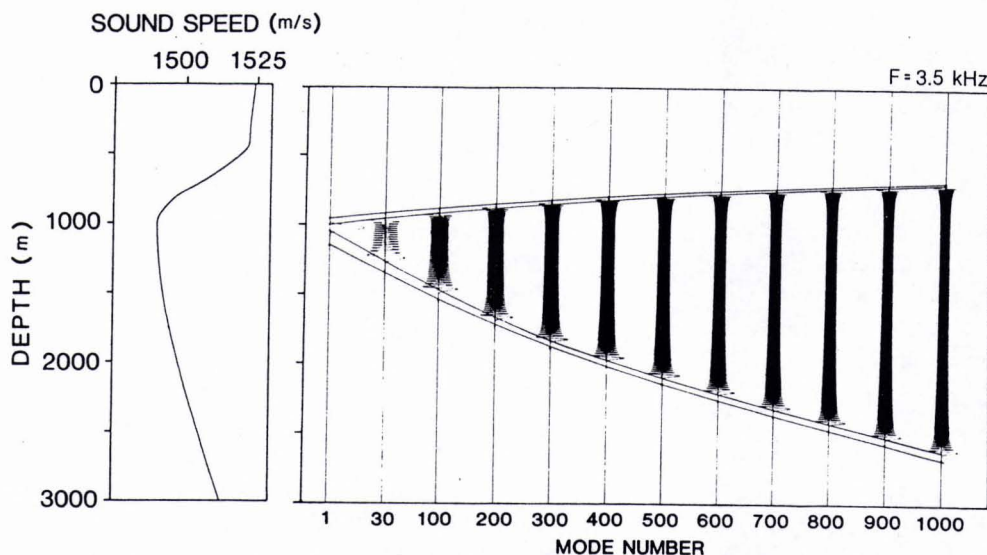
FIG. 1. Deep-water profile with associated mode functions.

at a depth of 1000 m, the axis of the sound channel of the profile shown in Fig. 1. Rays are calculated leaving the source with angles between ± 10°. Of course, the number of modes involved in the problem increases with beamwidth. We have here and in the following example limited the beamwidth in order to keep the total computing time within reasonable limits, though demonstrating that we are able to compute the lower-order modes, which are the most difficult modes to evaluate using standard mode programs. In the following comparison between ray-trace and normal-mode propagation-loss calculations we have neglected volume loss in both models for display purposes. Furthermore, knowing that the two models use different profile interpolations (curve fitting and linear) we have inputted about 400 profile points in order to ensure that the two models solve for the same environment.

Figure 3(a) shows the result with the source on the axis and the receiver at 2500-m depth. The dashed curve is the ray-theory result. If we return to Fig. 2 and follow the dashed line at 2500-m depth, we see that the shadow zones in Fig. 3(a) correspond to the regions where there are no rays. The normal-mode calculation shown in Fig. 3(a) results from summing the 1439 modes corresponding to the limiting angles of the rays leaving the source. Here we see that there is basically good agreement in high-intensity regions but that the ray calculation does not agree with the normal-mode wave-theory solution in the "shadow" regions, where wave

theory predicts a finite though low field level. Of course, there is a strong physical correspondence between the normal-mode result and the ray result. Hence, ray theory predicts, from Fig. 2, single-ray arrivals from 10 to 20 km and again from 30 to 40 km. The normal-mode result shows this by the lack of a distinct interference pattern in these regions. In the intermediate region from 20 to 30 km, we see from the ray trace that we are in a region of multiple arrivals, and hence we see the interference pattern in the normal-mode result. There is this one-to-one correspondence in all the results in Figs. 2 and 3.

On-axis calculations are also interesting. Figure 3(b) shows the corresponding results from normal-mode and ray calculations. Notice in Fig. 2 that there are no rays above the
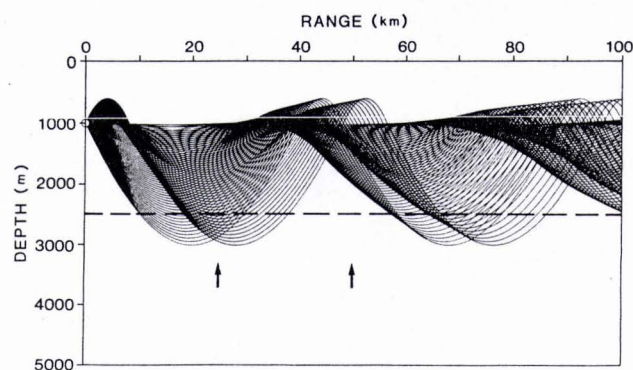

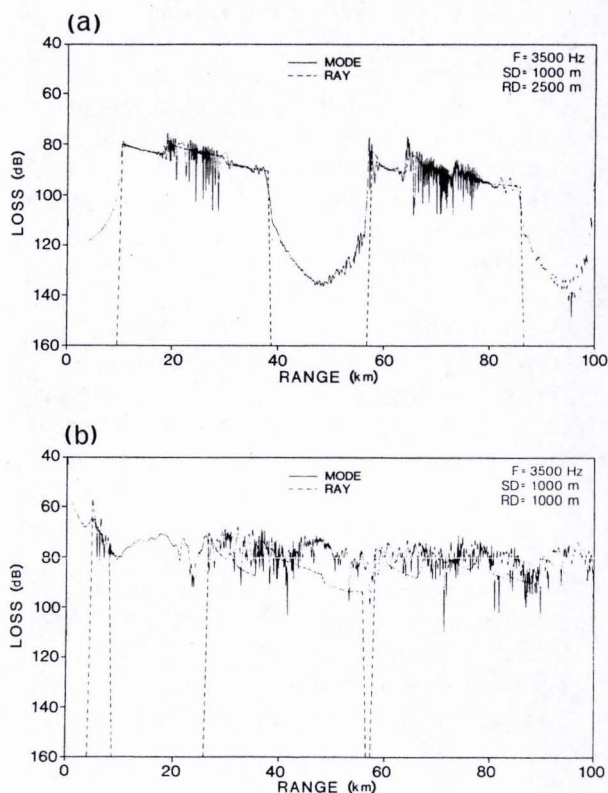FIG. 2. Ray trace for source on sound-channel axis (beamwidth is ± 10°).

FIG. 3. Propagation loss versus range for source on sound-channel axis. (a) Receiver below axis; (b) receiver on axis.
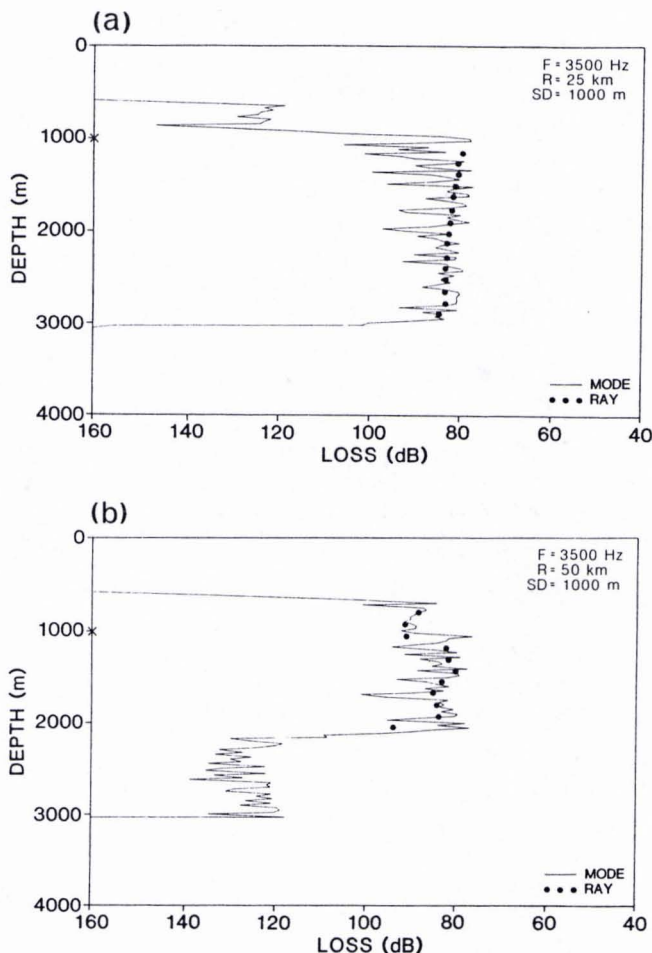
FIG. 4. Vertical distribution of the acoustic fields for source on sound-channel axis. (a) Range 25 km; (b) range 50 km.

sound-channel axis at ranges from about 10 to 30 km. In this range interval, the ray calculation predicts a sharp shadow zone (a ray trace artifact), whereas the finite-frequency wave-theory result does not show this feature. The agreement improves after 30 km when more of the water column is insonified above the sound-channel axis.

In Fig. 4 we compare the two types of calculations for the vertical distribution of the field at the two ranges (25 and 50 km) indicated by the arrows in Fig. 2. Again we see that in high-intensity regions the agreement is good, while only wave theory predicts some field intensity in the shadow regions.

II. COMPARISON WITH ANALYTIC RESULTS

The results presented in the last section were for a real ocean profile. There also exist profiles from which one can obtain analytic solutions to the ray equations. These solutions are valuable since they can be used to check numerical solutions. In this section we will compare our numerical solutions with the analytic solution for the parabolic profile

$$c(z) = c_0(1 + a^2z^2). \tag{2}$$

If θ_0 is the angle of emission of a ray from the source, then for small angles the trajectory of the ray can be analytically expressed to order θ_0^2 as[14]

$$z = (\theta_0/\sqrt{2}a) \sin(\sqrt{2}ar), \tag{3}$$

where θ_0 is in radians; r is range and hence there is perfect focusing at range multiples of

$$r_0 = \pi/\sqrt{2}a. \tag{4}$$

Notice also from Eq. (3) that for a given range, the depth z of a ray is directly proportional to θ_0 which means that rays are equally spaced as a function of depth. Hence the density of rays is constant over depth and therefore the intensity is constant over depth (for the small-angle approximation to order θ_0^2).

Figure 5(a) shows a ray trace for the source on the axis of the parabolic profile (the parameter "a" is 0.163 km^{-1} leading to a focal range of 13.6 km); the beamwidth is $\pm 4°$. Figure 5(b) is the contour of the field from a normal-mode calculation where we have limited the number of modes to correspond to the above beamwidth, i.e., the first 222 modes for a frequency of 5 kHz. To make the comparison easy, we have here taken out both volume attenuation and cylindrical spreading. We clearly see the focusing as described by Eq. (4). The vertical contour lines in Fig. 5(b), for the normal-mode computation, indicate constant intensity in the internal regions as a function of depth at a given range corresponding to the equal spacing of the rays in Fig. 5(a). The essential difference between the calculations is the finite-frequency effects of the normal-mode calculation, i.e., the degree of focusing, and that the decay of the field outside the insonified region is a function of frequency.

We can explicitly see this frequency effect by examining the field as a function of depth at a mid-cycle range and at a focal point. In Fig. 6 we plot the field at mid-cycle range (6.8 km) from 50 to 5000 Hz. Since the sound channel is symmetric around the source depth, only odd-number modes are excited (even-number modes have a null on the axis), and the curves in Fig. 6 result from adding 1, 2, 11, and 111 modes, respectively. We see that as we go to high frequency the intensity approaches a constant as a function of depth in agreement with ray theory, except at the edges. This edge effect is the well-known "Gibbs overshoot" phenomenon,
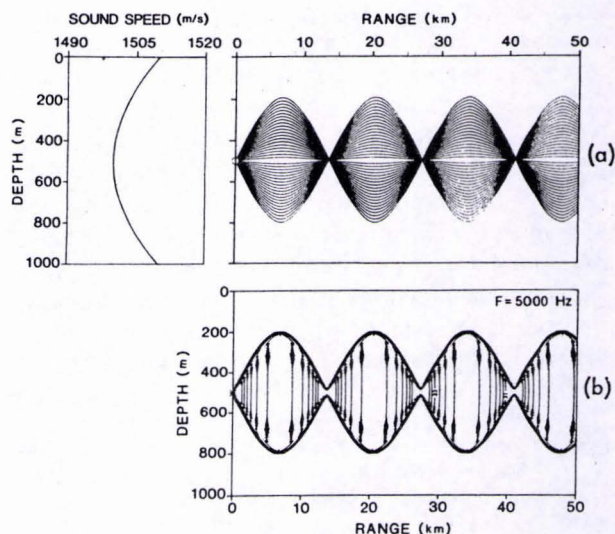

FIG. 5. Parabolic profile and associated ray trace (a) for source on sound-channel axis (beamwidth is $\pm 4°$); (b) corresponding propagation loss contours from normal-mode calculations.
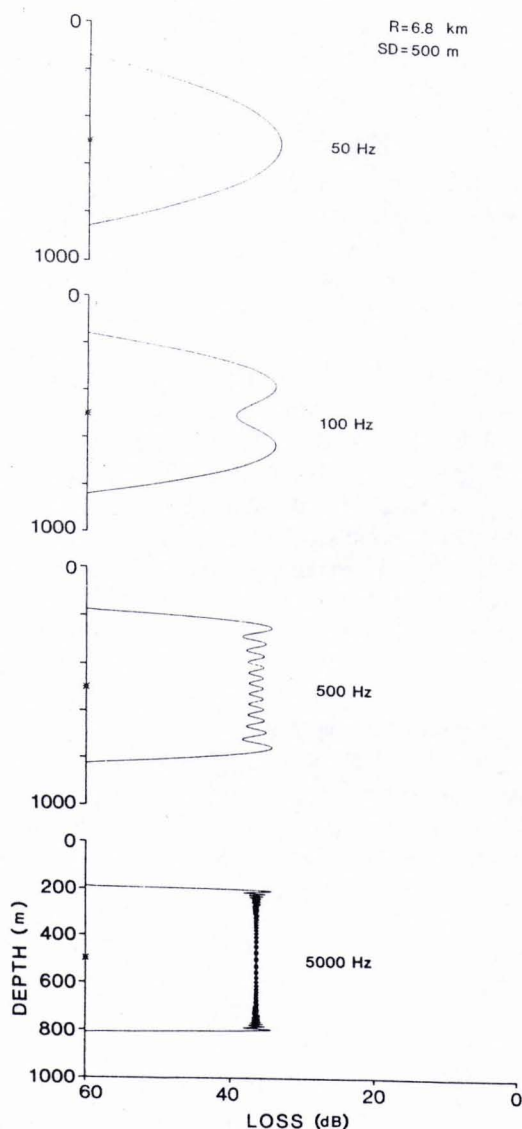
FIG. 6. Vertical distribution of acoustic field at mid-cycle range from mode calculations for parabolic profile.

which results when one tries to expand a function whose derivative is discontinuous (the ray result) in a sum of continuous functions (normal modes) with continuous derivatives.

The frequency dependence at the focal range is shown in Fig. 7. Notice that there is no focusing at 50 Hz, where the vertical distribution is equal at all ranges (see Figs. 6 and 7). With increasing frequency, wave theory predicts an increased focusing, though with a finite width and intensity at any finite frequency. Uncorrected ray theory, on the other hand, gives infinite focusing. Results similar to those presented here have been reported earlier[15,16] for normal-mode calculations using the analytic series expansion of the solution of the wave equation. The results presented in this paper are obtained from a numerical procedure that is not dependent on the existence of an exact analytic solution for a specific profile.

III. SUMMARY

We have presented a technique to perform high-frequency deep-water normal-mode calculations. We have

shown that it agrees in the high-frequency limit with ray theory, but we have also displayed the differences resulting from the wave nature of the normal-mode solution; these differences decrease as the wave theory is evaluated at higher frequencies. It is also known that this technique gives answers at lower frequencies that are identical to those from straightforward normal-mode calculations. Furthermore, we have obtained identical wave solutions to the high-frequency test problems of this paper using a fast field program[11,12] (FFP). Hence we are confident that the mode results presented here are accurate solutions of the wave equation. Though it is not yet practical to do normal-mode calculations at such high frequencies for "production runs," these calculations serve to provide a set of test cases that could be used to check whether other faster asymptotic techniques are correctly handling the frequency dependence of the acoustic field, especially around caustics and limiting rays.
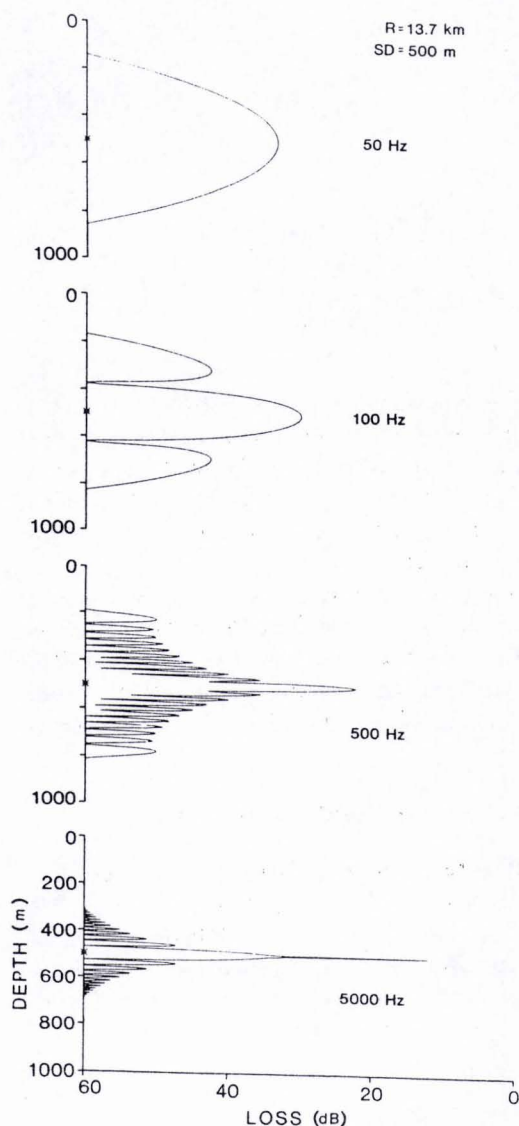

FIG. 7. Vertical distribution of acoustic field at focal range from mode calculations for parabolic profile.

ACKNOWLEDGMENT

[1] *Wave Propagation and Underwater Acoustics*, edited by J. B. Keller and J. S. Papadakis (Springer–Verlag, New York, 1977).

[2] V. M. Kudryashov, "Combination Normal Mode–Ray Technique for the Calculation of Sound Fields in Waveguides," Sov. Phys. Acoust. **22**, 406–408 (1976).

[3] L. B. Felsen, "Hybrid Ray-Mode Fields in Inhomogeneous Waveguides and Ducts," J. Acoust. Soc. Am. **69**, 352–361 (1981).

[4] R. Burridge and H. Weinberg, "Horizontal Rays and Vertical Modes," in *Wave Propagation and Underwater Acoustics*, edited by J. B. Keller and J. S. Papadakis (Springer–Verlag, New York, 1977), pp. 86–152.

[5] R. Laval and Y. Labasque, "Computations of Averaged Sound-Propagation Losses and Frequency/Space Coherence Functions in Shallow Waters," in *Bottom-Interacting Ocean Acoustics*, edited by W. A. Kuperman and F. B. Jensen (Plenum, New York, 1980), pp. 399–415.

[6] L. B. Dozier, "Calculation of Normal Modes in a Stratified Ocean," Science Applications, Inc., McLean, VA (1977) (unpublished).

[7] K. M. Guthrie, "Wave Theory of SOFAR Signal Shape," J. Acoust. Soc. Am. **56**, 827–836 (1974).

[8] F. B. Jensen and M. C. Ferla, "SNAP: the SACLANTCEN Normal-Mode Acoustic Propagation Model," Rep. SM–121, SACLANT ASW Research Centre, La Spezia, Italy (1979).

[9] F. B. Jensen and W. A. Kuperman, "Consistency Tests of Acoustic Propagation Models," Rep. SM–157, SACLANT ASW Research Centre, La Spezia, Italy (1982).

[10] M. C. Ferla, G. Dreini, F. B. Jensen, and W. A. Kuperman, "Broadband Model/Data Comparisons for Acoustic Propagation in Coastal Waters," in *Bottom-Interacting Ocean Acoustics*, edited by W. A. Kuperman and F. B. Jensen (Plenum, New York, 1980), pp. 577–592.

[11] F. R. DiNapoli, "Fast Field Program for Multilayered Media," Rep. 4103, Nav. Underwater Syst. Cent., New London, CT (1971).

[12] H. W. Kutschale, "Rapid Computation by Wave Theory of Propagation Loss in the Arctic Ocean," Rep. CU–8–73, Columbia Univ., Palisades, NY (1973).

[13] H. Weinberg, "Navy Interim Surface Ship Model (NISSM) II," Rep. TR–4527, Nav. Underwater Syst. Cent., New London, CT (1973).

[14] R. R. Goodman and L. R. B. Duykers, "Calculations of Convergent Zones in a Sound Channel," J. Acoust. Soc. Am. **34**, 960–962 (1962).

[15] N. C. Nicholas and H. Überall, "Normal-Mode Propagation Calculations for a Parabolic Velocity Profile," J. Acoust. Soc. Am. **48**, 745–752 (1970).

[16] R. D. Graves, A. Nagl, H. Überall, and G. L. Zarur, "Normal Modes in a Sound Channel with Range Dependent Parabolic Sound Speed Profile," Acustica **39**, 173–181 (1978).

INITIAL DISTRIBUTION

	Copies		Copies
MINISTRIES OF DEFENCE		**SCNR FOR SACLANTCEN**	
MOD Belgium	2	SCNR Belgium	1
DND Canada	10	SCNR Canada	1
CHOD Denmark	8	SCNR Denmark	1
MOD France	8	SCNR Germany	1
MOD Germany	15	SCNR Greece	1
MOD Greece	11	SCNR Italy	1
MOD Italy	10	SCNR Netherlands	1
MOD Netherlands	12	SCNR Norway	1
CHOD Norway	10	SCNR Portugal	1
MOD Portugal	5	SCNR Turkey	1
MOD Turkey	5	SCNR U.K.	1
MOD U.K.	16	SCNR U.S.	2
SECDEF U.S.	65	SECGEN Rep. SCNR	1
		NAMILCOM Rep. SCNR	1
NATO AUTHORITIES			
		NATIONAL LIAISON OFFICERS	
Defence Planning Committee	3	NLO Canada	1
NAMILCOM	2	NLO Denmark	1
SACLANT	10	NLO Germany	1
SACLANTREPEUR	1	NLO Italy	1
CINCWESTLANT/COMOCEANLANT	1	NLO U.K.	1
COMIBERLANT	1	NLO U.S.	1
CINCEASTLANT	1		
COMSUBACLANT	1	**NLR TO SACLANT**	
COMMAIREASTLANT	1		
SACEUR	2	NLR Belgium	1
CINCNORTH	1	NLR Canada	1
CINCSOUTH	1	NLR Denmark	1
COMNAVSOUTH	1	NLR Germany	1
COMSTRIKFORSOUTH	1	NLR Greece	1
COMEDCENT	1	NLR Italy	1
COMMARAIRMED	1	NLR Netherlands	1
CINCHAN	1	NLR Norway	1
		NLR Portugal	1
		NLR Turkey	1
		NLR UK	1
		NLR US	1
		Total initial distribution	240
		SACLANTCEN Library	10
		Stock	30
		Total number of copies	280